

Theoretical Investigation of the Periodic Anderson Hamiltonian of Samarium Hexaboride

**Partha Goswami and Udai Prakash Tyagi*

D.B.College, University of Delhi, Kalkaji, New Delhi-110019, India

**Email of the corresponding author: physicsgoswami@gmail.com*

Email of the second author: uptyagi@yahoo.co.in

Abstract

The periodic Anderson Hamiltonian of the bulk samarium hexaboride is investigated in this article assuming the presence of ferromagnetic impurities (FM). The problem of large on-site electron-electron repulsion is reformulated in terms of a holonomic constraint using slave-boson technique. The model analysis yields the possibility of the quantum anomalous Hall phase albeit with high integer value of the Chern number despite no band-crossing feature at discrete nodes as in 3D (Weyl) systems. Also, upon using the Fu-Kane-Mele formalism, it is shown that the surface Hamiltonian without FM corresponds to a strong topological insulator.

Keywords: Periodic Anderson Hamiltonian, Holonomic constraint, Slave-boson technique, Quantum anomalous Hall phase, Chern number, Fu-Kane-Mele formalism.

1.Introduction

The strong correlation effects and diverse surface conditions make a generic topological Kondo Insulator (TKI)[1-3]system, such as SmB_6 , extremely complicated - almost a Gordian knot [4-16]. This communication is on the compound SmB_6 —a narrow gap TKI which, with a high-temperature metallic phase, transforms into a paramagnetic charge insulator below 45 K. The fulcrum of our investigation of the compound is the periodic Anderson model (PAM) extended using the slave-boson (SB) formalism [3, 17,18]. It is shown that the proximity to the ferromagnetic magnetic (FM) impurities, which breaks time reversal symmetry (TRS), leads to the possibility of the quantum anomalous Hall (QAH) phase in the insulating bulk for certain parameter window(s) albeit with high integer value of the Chern number and non-integer values for metallic bulk. This happens despite no band-crossing feature at discrete nodes as in 3D (Weyl) systems [19]. The reason being along paths \mathcal{P} connecting high-symmetry points in the bulk Brillouin zone, which we will consider below, the z-component of the wave vector (ak_z) is either zero, or π . Thus, along \mathcal{P} there is ak_z -independence which implies that, effectively, we have a 2D system along these paths.

It has been suggested [1,2], as well as there is mounting evidence [20-22] during the past several years, that SmB_6 is a strong topological insulator. This has generated great deal of excitement in the condensed matter physics community and it still remains a matter of intense debate [23-24]. The supporting evidence for the TKI scenario [20-22] notwithstanding, there is no jury-verdict regarding the nature of the bulk and surface states of SmB_6 [23-25]. Upon using the extended

PAM (FM exchange energy $M = 0$) for surface, it is shown in the Fu-Kane framework [26-28] that the invariant $Z_2 = -1$. This implies strongly topological surface states (TSS) which is in disagreement with refs.[23,24]. In this context, it may be mentioned that signature of two-dimensional Fermi surfaces on (100) and (101) surface planes supporting the presence of TSS were obtained in the quantum oscillation experiments of Li et al. [29].

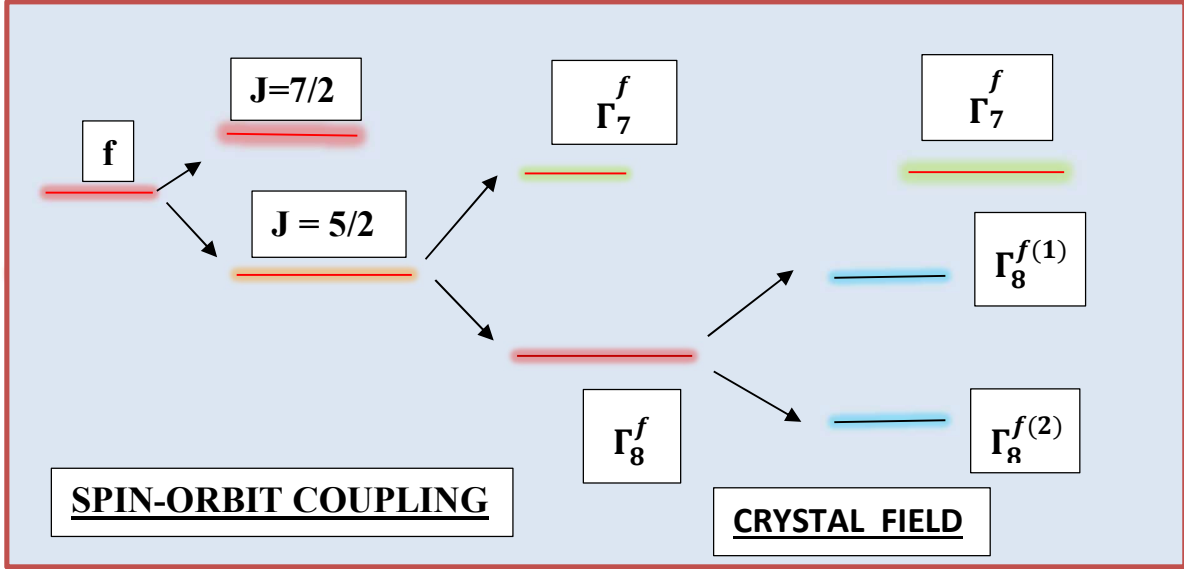


Figure 1. A representation of the evolution of energy levels of the f -states in SmB_6 owing to mediation of the spin-orbit coupling and the crystal field.

It was found earlier within the local density approximation + Gutzwiller method incorporating a Green's function scheme [16,30,31] that the states near the Fermi energy in SmB_6 are formed by the Sm 5d electrons (exhibiting t_{2g} and e_g symmetry) and the Sm 4f electrons. The f -states are split into $J = 7/2$ and $J = 5/2$ states by spin-orbit coupling. The $J = 5/2$ state is slightly below the Fermi energy E_F . It splits into Γ_7^f doublet and a Γ_8^f quartet due to presence of the crystal field (see Figure 1). The Γ_8^f quartet further splits into $\Gamma_8^{f(1)}$ and $\Gamma_8^{f(2)}$ doublets. On a quick side note, we shall denote below the fermionic operator creating a localized doublet state at a site \mathbf{r} , associated with the crystal field effect and spin-orbit coupling, by $f_{m_j}^\dagger(\mathbf{r})$. In the case of SmB_6 , the lowest-lying doublet is $|\Gamma_8^{f(2)}\rangle = |m_j = \pm \frac{1}{2}\rangle$, where $m_j = \pm \frac{1}{2}$ (or, $m_j = \uparrow, \downarrow$) is a pseudospin quantum number, corresponding to the two possible values of the projection of total angular momentum in this lowest-lying state. The hybridization between the d -electron operator $d_\tau^\dagger(\mathbf{r})$ (where $\tau (= \uparrow, \downarrow)$ is the spin index) and Γ^f operator $f_\alpha(\mathbf{r}')$ (where $\alpha = m_j$) are supposedly responsible for the opening of a larger gap $\Delta (\sim 20 \text{ meV})$ and a smaller one $\Delta' (\sim 3 \text{ meV})$ [30 – 34]. These complexities have been included in the earlier reports [30-34] as well as the present one to a certain degree. The energy dispersion obtained from this scheme is discussed in section 2 applying the SB- formalism.

The periodic Anderson model [3,17,18], which is the theoretical description of a Kondo insulator [35, 36] at the minimalistic level, is considered in sections 2 and 3. The model describes hybridization (V) between the conduction d -electrons (even parity) and localized, strongly-interacting f -electrons (odd parity) as already mentioned. The conduction electrons take care of the Kondo screening [37] of a localized magnetic moment. The nearest-neighbor (NN) hopping energy of these electrons $t_{d_1} \sim 25 \text{ meV}$. The NN hopping (t_{f_1}) of f -electrons may be assumed to be smaller than t_{d_1} . The correlation (U_f) of f -electrons is stronger on the surface than on the bulk. The topological order is due to V being comparable to the hopping energy of d -electrons, that is $V \sim t_{d_1} \sim 15 - 20 \text{ meV}$. In the opposite case, one obtains the Kondo lattice Hamiltonian [38]. The latter describes interaction between spins of localized and conduction electrons leading to Kondo singlet formation. This minimalistic SmB₆ (bulk) model [3,17,18], with $U_f \gg t_{d_1}$ and $V \sim t_{d_1}$, captures essential physics of TKI, such as the bulk and surface band-structure topology as shown in this report. The constraint $U_f \gg t_{d_1}$ imposes a non-holonomic constraint, viz. the exclusion of the double occupancy, which is very difficult to manipulate. The slave boson (SB)-framework provides here a platform to reformulate this nonholonomic constraint into a holonomic constraint.

The paper is organized as follows: In section 2, we obtain the bulk band spectrum in the SB formalism. Next, we calculate the Chern number to show the possibility of the quantum anomalous Hall (QAH) phase in the presence of FM. We obtain the surface state Hamiltonian in the absence of FM in section 3. We also calculate the Z_2 invariant using this within the Fu-Kane-Mele framework [26-28]. The highlights of the present work and the associated complexities are discussed in section 4 with very brief concluding remarks.

2. Model and Method

The minimalistic tight-binding Hamiltonian (PAM) [2,3,17] for the compound SmB₆ is given by

$$H_{PAM} = \sum_{k,\tau} E_k^d d_{k,\tau}^\dagger d_{k,\tau} + \sum_{k,\alpha} E_k^f f_{k,\alpha}^\dagger f_{k,\alpha} + \sum_{r,r'} \sum_{\alpha,\tau} \{F_{\alpha,\tau=\uparrow,\downarrow}(\mathbf{r}, \mathbf{r}') d_\tau^\dagger(\mathbf{r}) f_\alpha(\mathbf{r}') + \text{H.C.}\} \\ + U_f \sum_r \sum_{\alpha,\beta} f_\alpha^\dagger(\mathbf{r}) f_\alpha(\mathbf{r}) f_\beta^\dagger(\mathbf{r}) f_\beta(\mathbf{r}) \quad (1)$$

on a simple cubic lattice with the lattice constant a . The dispersions $E_k^d = -[2t_{d_1} c_1(k) + 4t_{d_2} c_2(k) + 8t_{d_3} c_3(k)]$ and $E_k^f = [-\epsilon_f - 2t_{f_1} c_1(k) - 4t_{f_2} c_2(k) - 8t_{f_3} c_3(k)]$ for d - and f -electrons, respectively, capture spread of atomic orbitals into bands. The terms (t_{d_1}, t_{f_1}) , (t_{d_2}, t_{f_2}) , and (t_{d_3}, t_{f_3}) , respectively, are the NN, NNN, and NNNN hopping parameters for d and f electrons (ϵ_f is the onsite energy of the f electrons), $c_1(k) = \sum_{j=(x,y,z)} \cos(ak_j)$, $c_2(k) = \sum_{i \neq j=(x,y,z)} \cos(ak_i) \cos(ak_j)$, and $c_3(k) = \prod_j \cos(ak_j)$. The annihilation operators for d -electron in momentum(\mathbf{k})-space is represented by $d_{k,\tau}$. The symbol U_f stands for the on-site repulsion among the f -electrons. Upon neglecting the spin-orbit coupling of d electrons, one may

regard the spin τ and the pseudo-spin index α as good quantum numbers prior to the hybridization represented by the term $F_{\alpha,\tau=\uparrow,\downarrow}(\mathbf{r},\mathbf{r}')$. Furthermore, the operator $f_\alpha(\mathbf{r})$ is related to the corresponding momentum space operator $f_{k,\alpha}$ by a simple Fourier transform $f_{k,\alpha} = \sum_{\mathbf{r}} \exp(-i\mathbf{k}\cdot\mathbf{r}) f_\alpha(\mathbf{r})$. Similarly, the Fourier transform of the hybridization parameter is $F_{\alpha,\tau}(\mathbf{k}) = \sum_{\mathbf{r},\mathbf{r}'} \exp(-i\mathbf{k}\cdot(\mathbf{r}-\mathbf{r}')) F_{\alpha,\tau=\uparrow,\downarrow}(\mathbf{r},\mathbf{r}')$. Since the f - and d -states have different parities, the momentum-dependent form-factor $F(\mathbf{k})$ involved in the third term in (1) must be odd. This is required in order to preserve time reversal symmetry (TRS), as the term involves coupling of the pseudo-spins with the physical spin of the electron. Therefore, in this article taking only the lowest-order cubic harmonics into account, we write this term as $2V(\mathbf{s}(k)\cdot\boldsymbol{\tau}')$, where V is the constant hybridization amplitude, $\mathbf{s}(k) = (\sin(ak_x), \sin(ak_y), \sin(ak_z))$, and $\boldsymbol{\tau}' = (\tau_x, \tau_y, \tau_z)$ are the Pauli matrices in spin space.

The extension of the mean-field-theoretic version of PAM [3,17,18] for a (topological) Kondo insulator is given below. As the first step of preliminaries, one makes the replacement $f_\alpha(\mathbf{r}) \rightarrow c_\alpha(\mathbf{r})b^\dagger(\mathbf{r})$ where $f_\alpha(\mathbf{r})$ is annihilation operator for an f -electron, $c_\alpha(\mathbf{r})$ is a spinful fermion annihilation operator, and $b^\dagger(\mathbf{r})$ is a spinless slave-boson creation operator at a site \mathbf{r} . The introduction of SB gives rise to extension in the Hilbert space of the system. The complications associated with the large on-site repulsion ($U_f \gg t_{d1}$) between the f -electrons, implying no double occupancy of a site, is then conveniently circumvented by imposing the holonomic constraint $[\sum_\alpha \langle c_\alpha^\dagger(\mathbf{r})c_\alpha(\mathbf{r}) \rangle + \langle b^\dagger(\mathbf{r})b(\mathbf{r}) \rangle] = 1$. As the next step, in order to simplify the problem, one assumes no spatial dependence of the boson operators and in addition replace them by their expectation value ($\langle b^\dagger(\mathbf{r})b(\mathbf{r}) \rangle \rightarrow |b|^2$). Here b may be complex as the density distribution of the bose-condensate is represented by a wavefunction with a well-defined amplitude and phase. Since one needs to recover the physical subspace of the extended Hilbert space, thus additionally $\sum_\alpha \langle f_\alpha^\dagger(\mathbf{r})f_\alpha(\mathbf{r}) \rangle = |b|^2 \sum_\alpha \langle c_\alpha^\dagger(\mathbf{r})c_\alpha(\mathbf{r}) \rangle$. The two of them put together, the constraint equation appears as $|b|^{-2} \sum_\alpha \langle f_\alpha^\dagger(\mathbf{r})f_\alpha(\mathbf{r}) \rangle = 1 - |b|^2$. With fluctuations of $(b^\dagger(\mathbf{r})b(\mathbf{r}))$ frozen, this holonomic constraint is then imposed in a mean-field fashion in ref.[3,17] using a Lagrange multiplier λ . For the formation of Kondo singlet states between f and d fermions one requires $N_c = N_d$, where N_c (N_d) correspond to the number of f - (d -) fermions. The auxiliary chemical potential ζ enforces the fact that there are equal number of f and d fermions. The minimization of the thermodynamic potential per unit volume leads to the self-consistent equations for λ and ζ . It is found [39] that $\lambda = -6t_{f1} + 6b^2t_{f1}$, $\xi = -3t_{d1} + 3t_{f1}$, where $t_{f1} < 0$ ($t_{f1} > 0$) for the insulating (conducting) bulk. The chemical potential μ of the fermion number enforces that $[\sum_{k,\alpha} \langle c_{\alpha,k}^\dagger c_{\alpha,k} \rangle + \sum_{k,\tau} \langle d_{k,\tau}^\dagger d_{k,\tau} \rangle]$ is the total number of fermions. The third step is to fix a reasonable value of the parameter $|b|$. For this purpose, the constraint-equation is considered once again. It appears as $\sum_{\alpha,ak < ak_F} \langle f_{k,\alpha}^\dagger f_{k,\alpha} \rangle = N(|b|^2 - |b|^4)$ where N is the total number of unit cells. In the low-temperature limit, the expectation value above needs to be replaced by the usual Heaviside step function. The multiplication of the Fermi momentum k_F with the lattice constant a yields a dimensionless quantity. The integration on the left-hand side is non-trivial, for assigning a single

value to the Fermi wave vector (ak_F) of an anisotropic (lattice) band structure whose Fermi surface(FS) may not be a sphere is inappropriate, However, as reported in refs. [40, 41], since there is formation of a large three dimensional (solely) conduction electron FS which takes place in the insulating bulk of SmB₆, one may lean on this mysterious finding to assume FS to be a sphere in the first approximation. This leads to the equation

$$|b|^2 = \left(\frac{1}{2}\right) \left[1 \pm \sqrt{\left(1 - \frac{\left(\frac{32\pi}{3}\right)(R^3 m_e^3 a^3 v_F^3)}{\hbar^3}\right)} \right], \quad (2)$$

where the relation $\hbar ak_F = m^* av_F$ has been used. The symbol v_F stands for the Fermi velocity $\sim 0.5 \times 10^3 \frac{m}{s}$ [27]. We shall give justification for using this value in section 3. The effective mass for electron is taken to be $m^* = Rm_e$ where m_e is the bare electron mass and $R > 1$ as the system is expected to have heavy fermions. In the Figure 2, plots of the two values of $|b|$, viz. $|b_1|$ and $|b_2|$, obtained from Eq.(1) as a function of R have been shown. In (a) $v_F = 0.5 \times 10^3 \frac{m}{s}$, while in (b) v_F is $1.0 \times 10^3 \frac{m}{s}$. It must be mentioned in this context that Q. Si et al. [42] have remarked that the Bose condensate part $\langle b^\dagger b \rangle$ rarely exceeds 0.25 in their investigation on competition between topological and Kondo insulator phases on a honeycomb lattice involving the same SB-methodology. We can see from Figure 2 that a value of $R \approx 160$ will yield two values of $|b|$, where one of them is nearly 0.5 and the other is nearly 0.9. The value of $|b|$ at which $|b_1|$ becomes equal to $|b_2|$ for the first time is $|b| \approx 0.7$ with $R \approx 175$. In the remaining part of the paper, this value of $|b|$ ($|b|^2 \approx 0.5$) will be used as contending with two values $|b|$ would then be avoided. Besides $|b|^2 \approx 0.50$ leads to integer Chern number for the insulator phase (see section 2) and reasonably satisfactory bulk band spectra. In order to obtain satisfactory surface band spectra, however, we need to have $|b|^2 \approx 0.70 - 0.80$. The corresponding value of the ratio

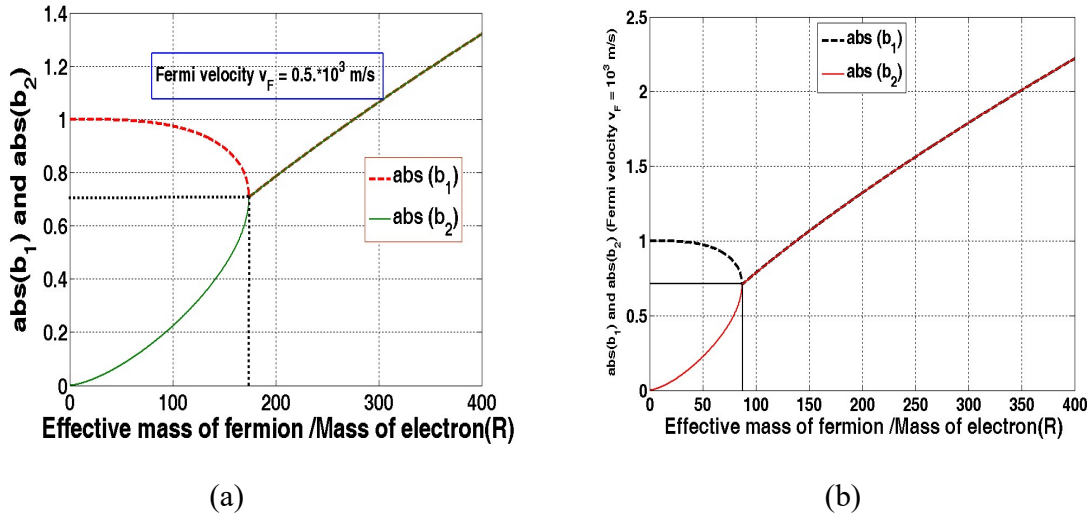


Figure 2. Plots of $|b_1|$ and $|b_2|$ as function of R for (a) $v_F = 0.5 \times 10^3 \frac{m}{s}$, and (b) $v_F = 1.0 \times 10^3 \frac{m}{s}$.

R is around 250 as one can see from Figure 2. In view of the scanning-tunnelling spectroscopic experimental result [43], where R was found to be 100-1000 for the surface states, our choice of $|b|^2 \approx 0.70 - 0.80$ for these states cannot be overruled.

The presence of the ferromagnetic magnetic impurities (FMI) in the 3 D system Hamiltonian is an additional feature. The impurities are assumed to be interacting with d electrons only. The magnitude of the impurity spin $|\mathbf{S}| > 1$ could be absorbed into the ferromagnetic coupling constant J and a term involving $M = |J| |\mathbf{S}|$ could be introduced. The constant term $\lambda N_c (|b|^2 - 1)$ in the Hamiltonian in [3,39] is omitted below. In the basis $(d_{k,\uparrow}^\dagger, d_{k,\downarrow}^\dagger, bc_{k,\uparrow}^\dagger, bc_{k,\downarrow}^\dagger)$, the mean-field theoretic SB Hamiltonian matrix could now be written as

$$h_{extended}(k, |b|, M) = \frac{\widetilde{E}_k^d(\mu)}{2} (\mathbb{I} + \gamma^0) + \frac{\widetilde{E}_k^f(\mu|b|)}{2} (\mathbb{I} - \gamma^0) + 2C_\mu \Sigma^\mu + \vartheta_\mu \gamma^0 \gamma^\mu. \quad (3)$$

Here \mathbb{I} is the identity matrix, $C_\mu = (0, 0, M)$, $\Sigma^\mu = \left(\frac{1}{2}\right) \epsilon^{\mu\nu\rho} \sigma_{\nu\rho}$, $\sigma_{\nu\rho} = \left(\frac{i}{2}\right) [\gamma_\nu, \gamma_\rho]$, and $\vartheta_\mu = (\vartheta_x, \vartheta_y, \vartheta_z)$. These components, respectively, are $\vartheta_x = 2V|b|\sin ak_x$, $\vartheta_y = 2V|b|\sin ak_y$, and $\vartheta_z = 2V|b|(\sin ak_z)$. The hybridization amplitude V is renormalized by $|b|$. The additional term $2C_\mu \Sigma^\mu$ breaks TRS. The Dirac matrices $(\gamma^0, \gamma^1, \gamma^2, \gamma^3, \gamma^5)$ in contravariant notations are $\gamma^0 = \tau^z \otimes I^{2 \times 2}$, $\gamma^j = i\tau^j \otimes \tau^j$, τ^i are Pauli matrices, $j = 1, 2, 3$, and $\gamma^5 = i\gamma^0 \gamma^1 \gamma^2 \gamma^3$. The renormalized dispersion of d - and f -electrons, respectively, are given by $\widetilde{E}_k^d(\mu) = -\mu - \xi + E_k^d$ and $\widetilde{E}_k^f(\mu, |b|) = -\mu + \xi + |b|^2 E_k^f + \lambda$. The hybridization bandgap $\Delta \sim 20 \text{ meV}$ is controlled by the energy scale $|b|V$ which must be of the same order of magnitude as Δ . As one can see from the SB protocol version of PAM given by Eq. (3), when $|b| \rightarrow 0$, the system is a non-interacting lattice gas mixture of itinerant d - and non-hopping f -fermions with no topological dispensation. The system shows the bulk metallic ($t_{f_1} > 0$) as well as the bulk insulating ($t_{f_1} < 0$) phases. The negative sign of t_{f_1} is also necessary for the band inversion, which induces the topological state [3]. Throughout the paper, we choose t_{d_1} to be the unit of energy. The eigen-values E_n of the Hamiltonian matrix $h_{extended}(k, |b|, M)$ in (3) are given by

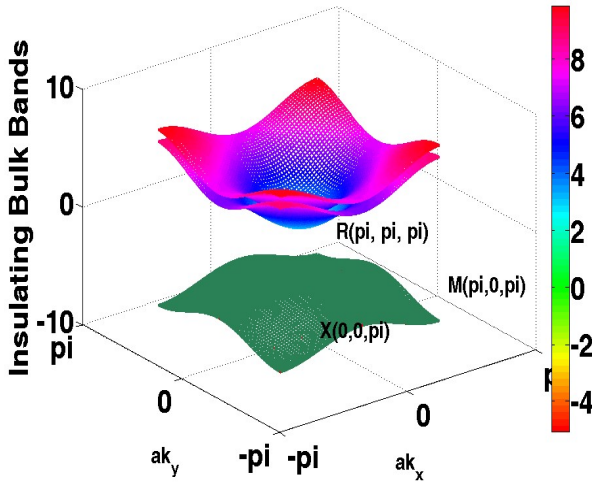
$$E_n(s, \tau, k, |b|, M) = \frac{(\widetilde{E}_k^d(\mu) + \widetilde{E}_k^f(\mu, b) + \tau M)}{2} + s \left[\frac{(\widetilde{E}_k^d(\mu) - \widetilde{E}_k^f(\mu, b) + \tau M)^2}{4} + \vartheta_x^2 + \vartheta_y^2 + \vartheta_z^2 \right]^{1/2} \quad (4)$$

where $n = 1, 2, 3, 4$, $\tau = \pm 1$ is the spin/pseudo-spin index and $s = \pm 1$ is the band-index. The bulk eigenstates corresponding to the eigenvalues in (4) are given in Appendix A.

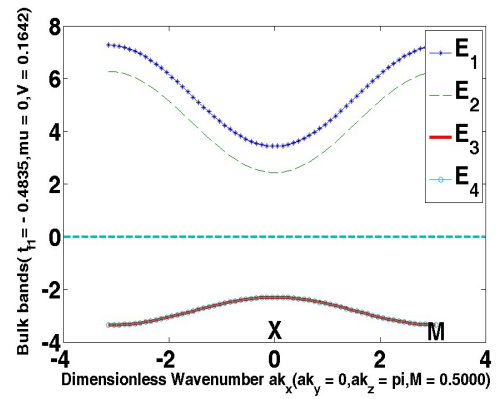
The high symmetry points (HSPs) of the bulk Brillouin zone (BZ) $\Gamma(0,0,0)$, $X\{(\pi, 0, 0), (0, \pi, 0), (0, 0, \pi)\}$, $M\{(\pi, \pi, 0), (\pi, 0, \pi), (0, \pi, \pi)\}$ and $R(\pi, \pi, \pi)$ are to be considered for plotting the single-particle spectra given by (4). The X and M points, three for each of them, are equivalent for symmetry reasons. We have plotted the bulk band energies of the system in Eq.(4) for $M \neq 0$ in Figure 3. The numerical values of the parameters used in the plots are $t_{d_1} = 1.0000$, $|t_{f_1}| = 0.4835$,

$t_{d_2} = 0.1, t_{f_2} = 0.1, t_{d_3} = 0.01, t_{f_3} = 0.01, \epsilon_f = -0.02, V = 0.1642, |b| = 0.7118, \mu = 0,$ and $M = 0.5000$. A 3D diagrammatic representation of the four bands (given by Eq.(4)) with spectral gap, due to $t_{f_1} < 0$, and $M \neq 0$, is shown in Figure 3(a). In (b) and (c), we have the plots of the same four bands as a function of the wave number component ak_x along the paths $\mathcal{P}: \bar{M}(-\pi, 0, \pi) - X(0, 0, \pi) - M(\pi, 0, \pi)$ and $\bar{R}(-\pi, \pi, \pi) - M(0, \pi, \pi) - R(\pi, \pi, \pi)$, respectively, with $t_{f_1} < 0$ (insulating bulk), and $M \neq 0$. The Fermi energy is represented by the horizontal line. The importance of the spectral gap in these figures cannot be overstated for the integer value of the Chern number \mathcal{C} to exist. In Figure 3(d), the plot of the four bands along the path $\bar{M}(-\pi, 0, \pi) - X(0, 0, \pi) - M(\pi, 0, \pi)$ is for the metallic bulk case ($t_{f_1} > 0$) where \mathcal{C} may have non-integer values. A 3D representation of the four bands showing no spectral gap (as $t_{f_1} > 0$) is shown in Figure 3(e). The spectra of the 3D system here display no band-crossing feature at discrete nodes as reported in 3D (Weyl) systems [19]. This was found to be essential for the Chern number \mathcal{C} to exist. We note that the terms $\vartheta_\mu \gamma^0 \gamma^\mu$ in (3) representing the hybridization are zero, and the re-normalized dispersion of d - and f -electrons are constant, at the HSPs. Besides, along the paths connecting HSPs mentioned above, the wave vector component $ak_z = 0$, or π . This means along these paths, effectively, we have a 2D system. The calculation of the intrinsic anomalous Hall conductivity (AHC)/Chern number (\mathcal{C}) below when $M \neq 0$ is, therefore, not infructuous.

The expression of AHC is $\sigma_{AH} = -\left(\frac{e^2}{h}\right) \sum_j \int_{BZ} \frac{d^2k}{(2\pi)^3} g(E_j(k) - \mu) \Omega_j^z(k)$, where μ is the chemical potential of the fermion number, j is the occupied band index, $g(E_j(k) - \mu)$ is the Fermi-



(a)



(b)

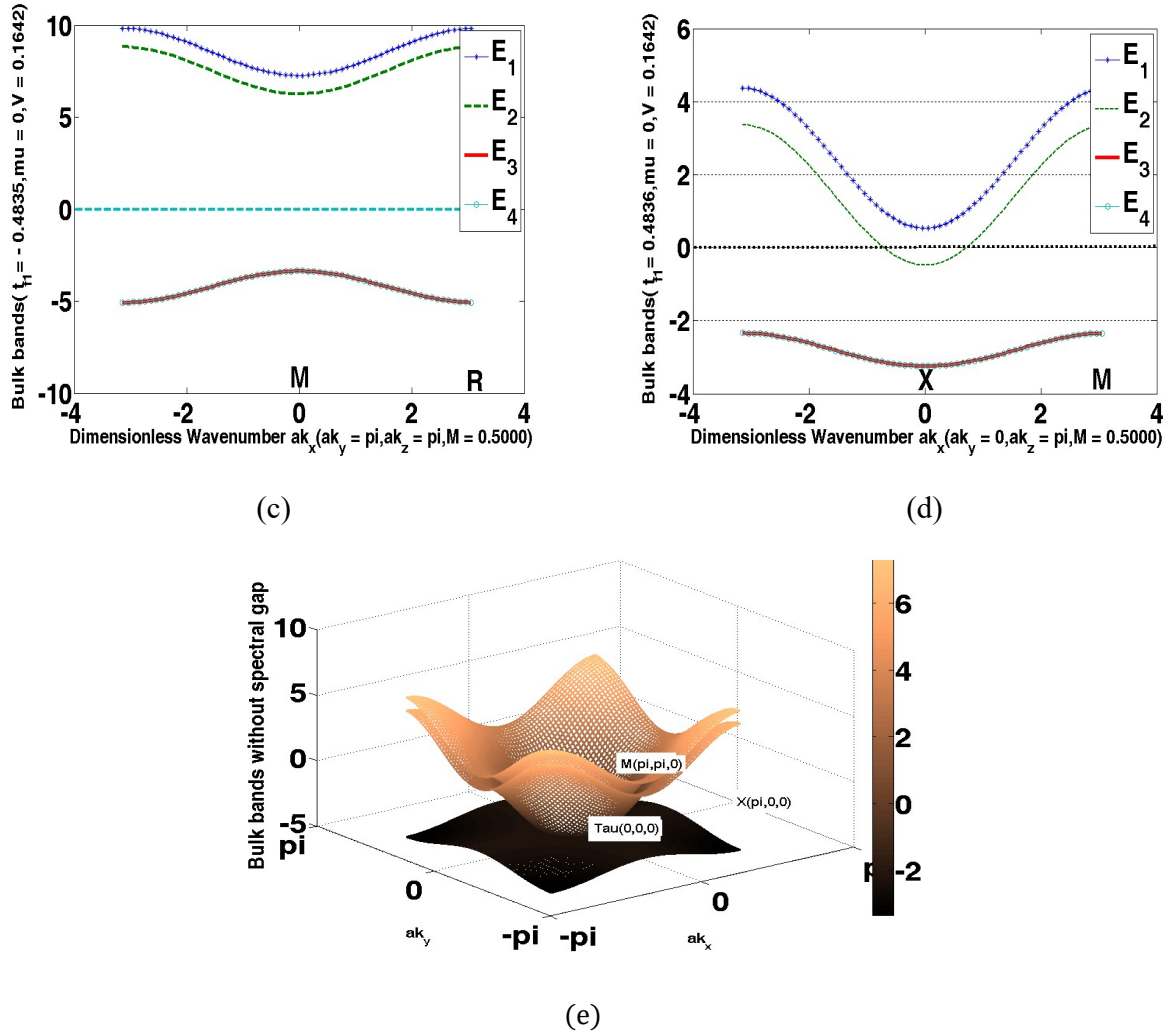


Figure 3. (a) A 3D diagrammatic representation of the four bands given by Eq.(4) with gap opening due to $t_{f_1} < 0$, and $M \neq 0$. (b) and (c) The representation of the same four bands along the paths $\bar{M}(-\pi, 0, \pi) - X(0, 0, \pi) - M(\pi, 0, \pi)$ and $\bar{R}(-\pi, \pi, \pi) - M(0, \pi, \pi) - R(\pi, \pi, \pi)$, respectively, with $t_{f_1} < 0$, and $M \neq 0$. (d) The plot of the four bands along the path $\bar{M}(-\pi, 0, \pi) - X(0, 0, \pi) - M(\pi, 0, \pi)$ for metallic bulk case ($t_{f_1} > 0$), and $M \neq 0$. (e) A 3D representation of the four bands showing no spectral gap as $t_{f_1} > 0$. The numerical values of the parameters used in the plots are $t_{d_1} = 1.0000$, $|t_{f_1}| = 0.4835$, $t_{d_2} = 0.1$, $t_{f_2} = 0.1$, $t_{d_3} = 0.01$, $t_{f_3} = 0.01$, $\epsilon_f = -0.02$, $V = 0.1642$, $b = 0.7118$, $\mu = 0$, and $M = 0.5000$. The Fermi energy is represented by the horizontal line.

Dirac distribution function and $\Omega_j^z(k)$ is the z -component of the Berry curvature (BC) for the j th band. To obtain AHC, we calculate BC using the Kubo formula

$$\Omega_j^z(k) = -2 \hbar^2 \left[\text{Im} \sum_{i \neq j} (E_j(k) - E_i(k))^{-2} \langle j, k | \widehat{v}_x | i, k \rangle \langle i, k | \widehat{v}_y | j, k \rangle \right]. \quad (5)$$

Here k is the Bloch wave vector, $E_j(k)$ is the band energy, $|j, k\rangle$ are the Bloch functions of a single band. The operator \widehat{v}_x represents the velocity in the x direction. For a system in a periodic potential

and its Bloch states as the eigenstates, in view of the Heisenberg equation of motion $i\hbar \frac{d\hat{x}}{dt} = [\hat{x}, \hat{H}]$, the identity $\langle m, \mathbf{k}' | \widehat{v}_\alpha | n, \mathbf{k} \rangle = \left(\frac{1}{\hbar}\right) (E_j(\mathbf{k}') - E_i(\mathbf{k})) \left\langle i, \mathbf{k}' \left| \frac{\partial}{\partial k_\alpha} \right| j, \mathbf{k} \right\rangle$ is satisfied. Upon using this identity, we obtain AHC in the zero temperature limit as $\sigma_{AH} = C \left(\frac{e^2}{\hbar}\right)$ where $C = \sum_j C_j$, $C_j = \int \int_{\text{BZ}} \Omega_j^z(k) \frac{d^2k}{(2\pi)^2}$. The z-component of the Berry-curvature(BC) is

$$\Omega^z(k) = \sum_j \left(\frac{\partial A_{j,y}}{\partial k_x} - \frac{\partial A_{j,x}}{\partial k_y} \right) = -2 \sum_j \text{Im} \left\langle \frac{\partial u_{j,k}}{\partial k_x} \left| \frac{\partial u_{j,k}}{\partial k_y} \right. \right\rangle \quad (6)$$

where $|u_{j,k}(k)\rangle = |j, k\rangle$. The vector potential $A_j(\mathbf{k})$ is the Berry connection and $\nabla_{\mathbf{k}} \times A_j(\mathbf{k}) = \Omega_j(\mathbf{k})$ is the Berry curvature (BC). We use the results presented in Eq. (6) to calculate BC. The high symmetry points (HSPs) of the bulk Brillouin zone (BZ) are given above. In line with the bulk-boundary correspondence, upon considering these points and the eigenvectors of the bulk system in the Appendix A, BC is calculated analytically ensuring that all occupied levels are taken in. Next, on integrating BC on a k-mesh-grid (with appropriate resolution) of the Brillouin zone, we calculate the intrinsic AHC. We use the ‘Mat-lab’ package for this purpose. The grids are created by the command $[x, y] = \text{mesh-grid}([- \pi : \varepsilon : + \pi])$ where the parameter ε takes care of the number (N) of grids. For example, $\varepsilon = 0.06$ yields $N = 11025$. Finally, the command $C_m = N^{-1} \text{sum}(\text{sum}(BZ_n))$, where BZ_n is BC value on n^{th} grid, is required to obtain the Chern number $\mathcal{C} = \sum_m C_m$. Here ‘m’ The contour plots of BC are given in Figure 4(a) - 4(d). The numerical values of the parameters to be used are obtained by trial- and- error method. In the plots 4(a) and 4(b), for example, these are the same as those in Figure 3. Whereas $t_{f_1} < 0$ for the Figure 4(a), it is positive for 4(b). The chern number calculated in the two cases are **(a)** $\mathcal{C} = -7.0003 \sim -7$, **(b)** $\mathcal{C} = 5.9685$ (metallic bulk). Interestingly, the chern number calculated in the other two cases are **(c)** $\mathcal{C} = -2.0043 \sim -2$, and **(d)** $\mathcal{C} = 2.0073 \sim +2$ for a higher value of $|b| (= 0.90)$. The numerical values of the parameters used in the plots are $t_{d_1} = 1$, $t_{f_1} = -0.5$, $t_{d_2} = 0.1$, $t_{f_2} = 0.1$, $t_{d_3} = 0.01$, $t_{f_3} = 0.01$, $\varepsilon_f = -0.02$, and $\mu = 0$. and $M = 0.10$. The additional parameter values in **(c)** $ak_z = \pi$, $t_{f_1} = -0.515$, $V = 0.50$, and $M = 0.20$, while in **(d)** $ak_z = 0$, $t_{f_1} = -0.491$, $V = 0.620$, and $M = 0.10$. It may be noted that in this case the hybridization parameter is under-renormalized. A positive (negative) Chern number implies that the unidirectional edge waves propagate clockwise (anti-clockwise) with respect to the z-axis. We, thus, find a possibility for the insulator system investigated by the Hamiltonian (3) to be in the QAH phase when $M \neq 0$.

3. Z_2 invariant for $M=0$

We follow the well-known Fu and Kane [13] methodology based upon the eigenvalues of the parity operator for the purpose of calculating the Z_2 invariant when the exchange energy $M = 0$. We summarize the procedure in brief after obtaining the surface state band spectrum in our slave-boson formalism. We use an ansatz-based technique, similar in spirit to that in ref.[44], to obtain

the surface state Hamiltonian ($h_{\text{surface}}(k, \mu, |b|, M = 0)$). The ansatz corresponds to looking for evanescent states, almost localized within the surface $z = 0$, of the form $Ae^{-q} |u_n(k_x, k_y, k_z)\rangle$ for $z > 0$ and $Ae^{qz} |u_n(k_x, k_y, k_z)\rangle$ for $z < 0$, where $|u_n\rangle$ is given in Appendix A. The evanescent states are, thus, decaying for $z > 0$ and $z < 0$ if A is constant. For $A =$

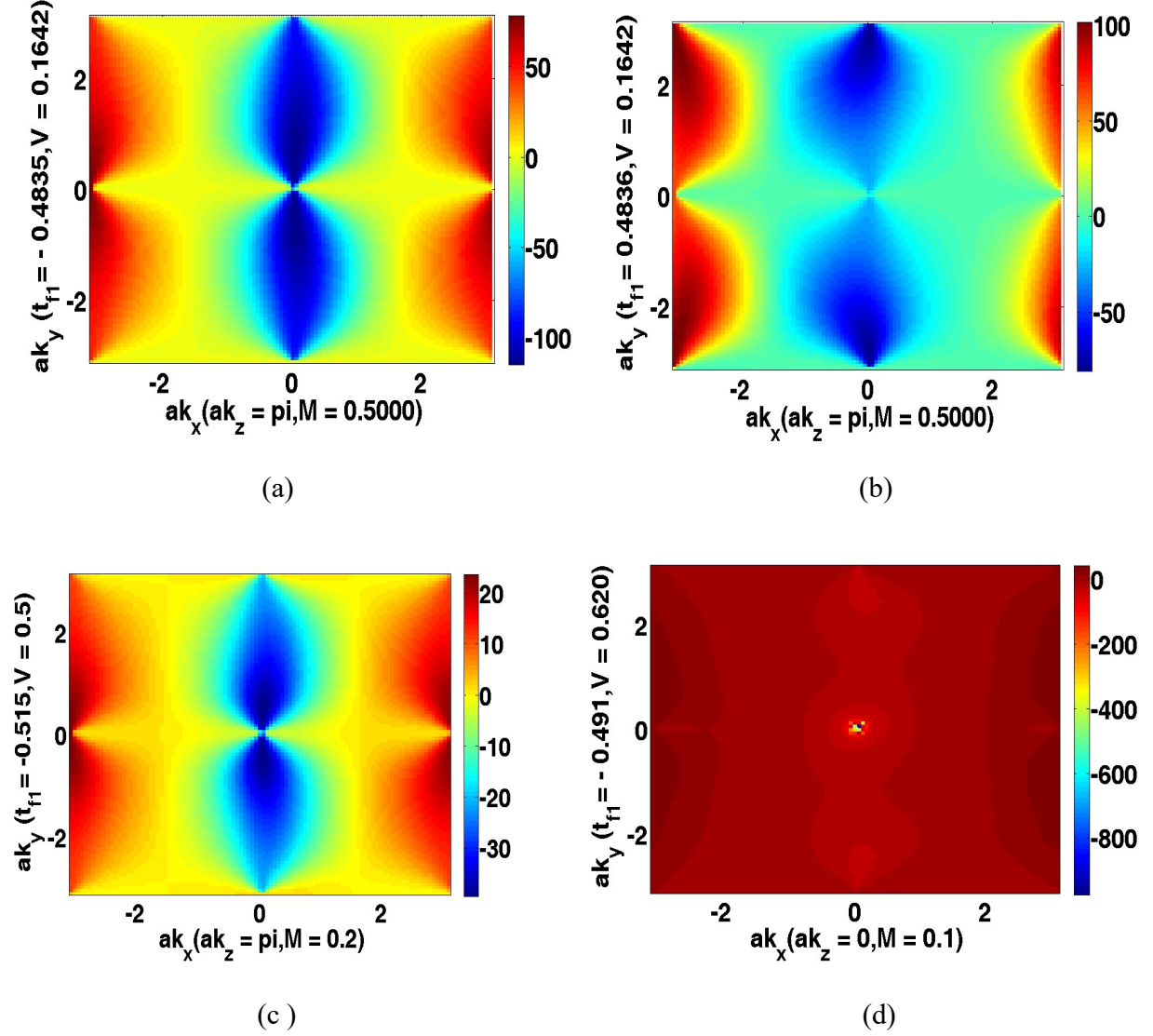


Figure 4. The contour plots of the Berry-curvature in the z -direction as a function of the dimension-less wave vector components ak_x and ak_y . The numerical values of the parameters used in the plots are the same as in Figure 3. In (a) $t_{f_1} < 0$, while in (b) $t_{f_1} > 0$. The chern number calculated in the two cases are (a) $\mathcal{C} = -7.0003 \sim -7$, and (b) $\mathcal{C} = 5.9685$. The numerical values of the parameters used in the plots in (c) and (d) are $t_{d_1} = 1, t_{f_1} = -0.5, t_{d_2} = 0.1, t_{f_2} = 0.1, t_{d_3} = 0.01, t_{f_3} = 0.01, \epsilon_f = -0.02$, and $\mu = 0$. The additional parameter values in (c) $ak_z = \pi, t_{f_1} = -0.515, V = 0.50$, and $M = 0.20$, while in (d) $ak_z = 0, t_{f_1} = -0.491, V = 0.620$, and $M = 0.10$. The chern number calculated in the two cases are (a) $\mathcal{C} = -2.0043 \sim -2$, and (b) $\mathcal{C} = 2.0073 \sim +2$.

$\cos(qz)$ as in [44], the states will be oscillatory in space with decaying amplitude. As the second step, we make the replacement $ak_z \rightarrow -ia\partial_z$ in the terms involving $\sin(ak_z)$ and $\cos(ak_z)$ in (3) to make them appear as polynomial operators $f(\partial_z)$ by using Taylor expansion. The third step is to use the substitution rule $f(\partial_z)e^{qz} = f(q)e^{qz}$. For $A = \cos(qz)$, the exponential-shift rule $f(\partial_z)e^{qz}u = e^{qz}f(\partial_z + q)u$ may be used. We take $A = 1$, for simplicity. Here ‘ q ’ is a wavenumber such that $q^{-1} \sim d$, where d is a depth introduced to facilitate the estimation of the surface state penetration. If we put the restriction that the surface state possesses the value $d \sim 5\text{-}10$ nm, we obtain $aq \sim 0.08 - 0.04$. This ensures that the decaying term $e^{-q|z|} \sim e^{-1}$ for $|z| \sim 5\text{-}10$ nm. This value of the penetration depth is comparable to that of Bi_2Se_3 . On the other hand, for the much lower value $d \sim 0.13$ nm, we obtain $aq \sim 3.1416 \dots \sim \pi$. Consequently, $e^{-q|z|}$ will be nearly equal to e^{-1} for very low value of $|z|$ ($\sim 0.1\text{nm}$). An intermediate value of the penetration depth $\sim 0.4\text{-}0.5$ nm will be considered below which corresponds to $aq \sim 1$. With these preliminaries, in the basis $(d_{k,\uparrow} \quad bc_{k,\downarrow} \quad d_{k,\downarrow} \quad bc_{k,\uparrow})^T$, the surface Hamiltonian may be written as

$$h_{\text{surface}}(k, \mu, |b|, q) = (\epsilon_0(k, \mu, b))\sigma_0 \otimes \tau_0 - \vartheta_x \sigma_x \otimes \tau_x - \vartheta_y \sigma_y \otimes \tau_y + \epsilon(k, \mu, b) \sigma_0 \otimes \tau_z \\ + \left(\frac{1}{2}\right) [-i \vartheta_{z0} (\sigma_x + i\sigma_y) \otimes \tau_z + i \vartheta_{z0} (\sigma_x - i\sigma_y) \otimes \tau_x], \quad (7)$$

where

$$\epsilon_0(k, \mu, b, q) = \frac{(\widetilde{E}_k^d(\mu, q) + \widetilde{E}_k^f(\mu, b, q))}{2}, \epsilon(k, \mu, b) = \frac{(\widetilde{E}_k^d(\mu, q) - \widetilde{E}_k^f(\mu, b, q))}{2}, \vartheta_{z0} = 2Vb \sin aq. \quad (8)$$

The Pauli matrices σ and τ are acting in the space of bands that give rise to Kramers degeneracy (see Figure 5 below). On a quick side note, it is perhaps worth mentioning that, in the very low penetration depth case, the Hamiltonian above could be written as

$$h_{\text{surface}}(k, \mu, |b|, M = 0) = \begin{pmatrix} \mathfrak{h}_+ = \mathfrak{h}((k_x, k_y, q, \mu, b)) & 0 \\ 0 & \mathfrak{h}_- = \mathfrak{h}^*(-k_x, -k_y, q, \mu, b) \end{pmatrix} \quad (9)$$

where $\mathfrak{h}_+ = (\epsilon(k, \mu, b))\tau_0 + \mathbf{n}(k_x, k_y, b) \cdot \boldsymbol{\tau}$, the two blocks $(\mathfrak{h}_+, \mathfrak{h}_-)$, characterized by the pseudo-spin indices $(+, -)$, are related to each other by time reversal symmetry (TRS), and $\mathbf{n}(k_x, k_y, q, b) = (-\vartheta_x, -\vartheta_y, \epsilon_0(k_x, k_y, \mu, b))$. Equation (9) corresponds to Qi-Wu-Zhang (QWZ) model [45-47]. As shown by these authors, the situation corresponds to the quantum spin Hall (QSH) state, for the spin Hall conductance of $\mathfrak{h}((k_x, k_y, q, \mu, b))$ and $\mathfrak{h}^*(-k_x, -k_y, q, \mu, b)$ are not zero but the net Hall conductance of the system described by Eq.(13) is zero. We shall, however, assume $aq \sim 1$ for the graphical representations below.

The eigenvalues E_n ($n = 5, 6, 7, 8$) of $h_{\text{surface}}(k, \mu, b, q)$ in (7) is given by a quartic $E_n^4 + a E_n^3 + b E_n^2 + c E_n + d = 0$. The coefficients (a, b, c, d) are given by $a = -2(\widetilde{E}_k^d(\mu, k) + \widetilde{E}_k^f(\mu, b, k))$, $b =$

$$\{(\widetilde{E}_k^d(\mu, k) + \widetilde{E}_k^f(\mu, b, k))^2 - M^2 + 2C^2\}, C^2 = (\widetilde{E}_k^d(\mu, k) \times \widetilde{E}_k^f(\mu, b, k)) - \vartheta_{z_0}^2 + (\vartheta_x^2 + \vartheta_y^2), c = \left\{ M^2 \widetilde{E}_k^f(\mu, b, k) - C^2 (\widetilde{E}_k^d(\mu, k) + \widetilde{E}_k^f(\mu, k, b)) \right\}, d = -M^2 \times \widetilde{E}_k^f(\mu, b, k) + C^4 - 4 \vartheta_{z_0}^2 (\vartheta_x^2 + \vartheta_y^2). \text{In}$$

view of the Ferrari's solution of a quartic equation, we find the roots as

$$E_n(s, \sigma, k, b) = \sigma \sqrt{\frac{\eta_0(k)}{2} - \frac{a}{4}} + s \left(b_0(k) - \left(\frac{\eta_0(k)}{2} \right) + \sigma c_0(k) \sqrt{\frac{2}{\eta_0(k)}} \right)^{\frac{1}{2}}, \quad (10)$$

where $\sigma = \pm 1$ is the spin index and $s = \pm 1$ is the band-index. The functions appearing in Eq. (16) are given by

$$\eta_0(k) = \frac{2b_0(k)}{3} + (\Delta(k) - \Delta_0(k))^{\frac{1}{3}} - (\Delta(k) + \Delta_0(k))^{\frac{1}{3}}, \quad \Delta_0(k) = \left(\frac{b_0^3(k)}{27} - \frac{b_0(k)d_0(k)}{3} - c_0^2(k) \right), \quad (11)$$

$$\Delta(k) = \left(\frac{2}{729} b_0^6 + \frac{4d_0^2 b_0^2}{27} + c_0^4 - \frac{d_0 b_0^4}{81} - \frac{2b_0^3}{27} + \frac{2c_0^2 b_0 d_0}{3} + \frac{d_0^3}{27} \right)^{1/2}, \quad b_0(k) = \left\{ \frac{3a^2 - 8b}{16} \right\}, \quad (12)$$

$$c_0(k) = \left\{ \frac{-a^3 + 4ab - 8c}{32} \right\}, \quad d_0(k) = \frac{-3a^4 + 256d - 64ac + 1}{256} \frac{2b}{1}. \quad (13)$$

We have plotted the surface state energy spectra (SSES) E_n ($n = 5, 6, 7, 8$) given by Eq. (10) as function of the dimensionless wave vector component ak_x in Figure 5. The curves in 5(a) correspond to the path $\Gamma(0,0,0) - X(\pi,0,0) - M(\pi,\pi,0)$. The Fermi energy is represented by the horizontal solid line. The curves (E_6, E_7) intersect the Fermi energy close to the point X indicated by a vertical line in 5(a). The curves (E_6, E_7) also display the band-inversion along the path $\Gamma(0,0,0) - X(\pi,0,0)$. In 5(b) we have plotted E_n ($n = 5, 6, 7, 8$) as a function of the wave number component ak_x along the path $\bar{X}(-\pi,0,0) - \Gamma(0,0,0) - X(\pi,0,0)$. The numerical values of the parameters used in all the plots are $t_{d_1} = 1.0000$, $|t_{f_1}| = 0.4835$, $t_{d_2} = 0.1$, $t_{f_2} = 0.1$, $t_{d_3} = 0.01$, $t_{f_3} = 0.01$, $\epsilon_f = -0.02$, $V = 0.1642$, $b = 0.7118$, $\mu = 0$, and $M = 0$. In all the three figures, t_{f_1} is negative and, therefore, the figures correspond to the insulating bulk. The presence of partially empty conduction band in (a) and (c) clearly indicates the presence of conducting surface state. In Figure 5(b), there is a Kramers degeneracy pair at $ak = (\pm 3, 0, 0)$ (indicated by vertical lines) as the pair satisfy the condition $ak + aG = -ak$ where aG is reciprocal lattice vector. There is band-touching at $ak_x = 0$ as well. The Dirac-cone feature (DCF) of surface state excitation spectrum connecting the valence band with the conduction band has been reported in earlier [48] at the Γ point. This was observed in several experiments, viz. by scanning-tunneling microscopy [49,50], angle-resolved photoemission spectroscopy (ARPES) [51,52], the circular dichroism ARPES [53], and so on. This feature is absent here as the linearization of the surface Hamiltonian matrix (7) has not been carried out around $\Gamma(0,0,0)$. Interestingly, upon treating the Hamiltonian (7) in the long-wavelength limit where the replacements

$$\sin(ak_j) \rightarrow ak_j + O(a^3 k_j^3), \quad \cos(ak_j) \rightarrow \left(1 - \frac{1}{2} a^2 k_j^2 \right) + O(a^4 k_j^4) \quad (14)$$

are necessary ($j = (x, y)$), using the parameter values $t_{d_1} = 1$, $t_{f_1} = -0.8$, $t_{d_2} = 0.01$, $t_{f_2} = 0.01$, $t_{d_3} = 0.001$, $t_{f_3} = 0.001$, $\epsilon_f = -0.02$, $V = 0.1$, $|b|^2 = 0.81$, and $\mu = 0$, access to the Dirac -

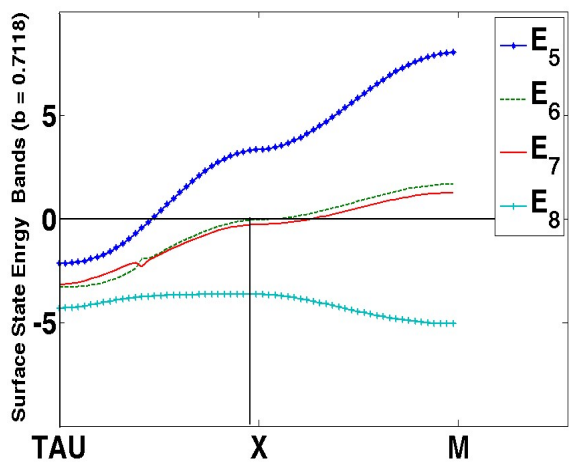
cone like feature (DCF) is possible as shown in the inset in 5(b). The value of $|b|^2$ as high as 0.81, however, corresponds to under re-normalization of the bare hybridization parameter and the dispersion of f -electrons. On the other hand, as we have explained in section 2, in view of the scanning-tunnelling spectroscopic experimental result [43] our choice of $|b|^2 \approx 0.80 - 0.90$ could not be overridden. The value of the Fermi velocity calculated (using the formula $\hbar^{-1}(\partial E/\partial k)$) with this choice of $|b|^2$ is nearly the same as what has been used in Figure 2. The DC – like feature is also displayed in Figure 5(c) and 5(d) at the time reversal invariant momenta (TRIM) $a\mathbf{k} = (\pm 1, 0, 0)$ for $|b|^2 \approx 0.89$ using the same procedure outlined in (14). In these plots the parameter values are $t_{d_1} = 1$, $t_{f_1} = -0.7900$, $t_{d_2} = 0.01$, $t_{f_2} = 0.01$, $t_{d_3} = 0.001$, $t_{f_3} = 0.001$, $\epsilon_f = -0.02$, $V = 0.1860$, $\mu = 0$, and $M = 0$. It must be mentioned that non-linear structure in these figures hint at the possibility of hosting massive Dirac fermions. The important lesson from these graphical representations is that the strong f -electron correlation in the bulk seems to lead to large effective mass of the carriers on the surface [43]. The z-component of the spin polarization density (or the spin texture) has also been calculated (see Appendix B for an outline) as function of (ak_x, ak_y) and displayed in 5(e) using the same parameter values except that $\mu = -0.01$. The representation indicates that there is a tiny pocket around Γ point where the electron spin polarization (locked to the momentum) is very high. There is a smaller spike too in the fourth quadrant of the zone. The DC-like feature and the spike in the spin polarization density are in favor of the fact that the surface state is topologically non-trivial. We seek further corroboration of the non-triviality by the analysis given below.

The appearance of topologically-protected surface states is the physical consequence of the nontriviality. Now the time reversal (TR) operator for a spin 1/2 particle is $\Theta = I^{2 \times 2} \otimes \tau^y K$. The operator K stands for the complex conjugation. The inversion symmetry (IS) operator, on the other hand, is constructed as $\Pi = I^{2 \times 2} \otimes \tau^z$. The τ^j are Pauli matrices on two-dimensional spin space. The Hamiltonian under consideration, for $M = 0$, preserves the time reversal (TRS) and inversion symmetries (IS). It can be easily shown that $\langle \Theta \psi | \Theta \varphi \rangle = \langle \varphi | \psi \rangle$ taking eigenstate of the z-component of the spin operator $I^{2 \times 2} \otimes \tau^z$ as the basis. Also, $\Theta \gamma^0 \Theta^{-1} = \gamma^0$, $\Theta \gamma^1 \Theta^{-1} = -\gamma^1$, and $\Theta \gamma^j \Theta^{-1} = \gamma^j$, where $j = 2, 3$. Similarly, $\Pi \gamma^0 \Pi^{-1} = \gamma^0$, $\Pi \gamma^j \Pi^{-1} = -\gamma^j$ ($j = 1, 2$), and $\Pi \gamma^k \Pi^{-1} = \gamma^k$ ($k = 3, 5$). Since only γ^0 , and γ^3 are even under time reversal and inversion, at a time reversal invariant momentum (TRIM) K_i where the system preserves both TR and IS, the Hamiltonian (7) will have the following form:

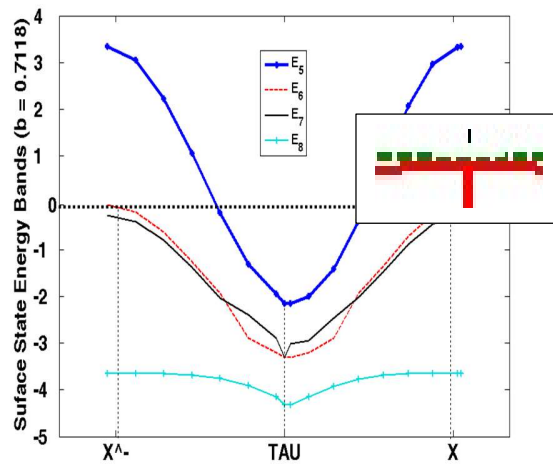
$$h_{\text{surface}}(k = K_i, M = 0) = \left[\frac{\widetilde{E}_k^d(\mu, k) + \widetilde{E}_k^f(\mu, b, k)}{2} \mathbb{I} + \frac{\widetilde{E}_k^d(\mu, k) - \widetilde{E}_k^f(\mu, b, k)}{2} \gamma^0 + \vartheta_{z0} \gamma^0 \gamma^3 \right]. \quad (15)$$

The eigenvalues of Π, γ^0 and $\gamma^0 \gamma^3$ are ± 1 (multiplicity 2). The eigenvectors corresponding to the eigenvalues $+1$ and -1 of the parity operator, respectively, are $|+\rangle = (1/\sqrt{2})(1 \ 0 \ 1 \ 0)^T$ and $|-\rangle = (1/\sqrt{2})(0 \ -1 \ 0 \ -1)^T$. These are the relevant eigenstates. It is easy to see that

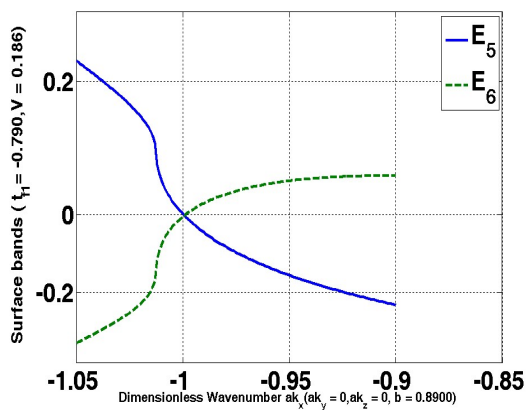
$$\langle + | h_{\text{surface}}(k = K_i, M = 0) | + \rangle = \widetilde{E}_k^d(\mu, k) + \vartheta_{z0} = E_+, \quad (16)$$



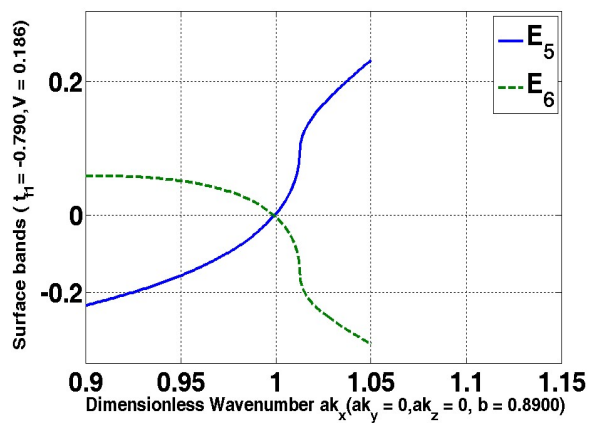
(a)



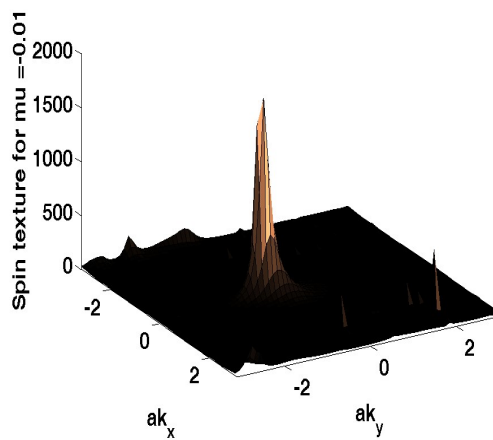
(b)



(c)



(d)



(e)

Figure 5. The plots of the surface band energies (Eq. (10)) when the bulk is insulator. The partially empty bands show that the surface is conducting. The numerical values of the parameters used in the plots in (a) and (b) are the same as in Figure 3. The Fermi energy is represented by the horizontal solid line. The numerical values of the parameters used in the inset are $t_{d_1} = 1$, $t_{f_1} = -0.8$, $t_{d_2} = 0.01$, $t_{f_2} = 0.01$, $t_{d_3} = 0.001$, $t_{f_3} = 0.001$, $\epsilon_f = -0.02$, $V = 0.1$, $|b| = 0.98$, $\mu = 0$, and $M = 0$, where the Dirac cone like feature is at $\mathbf{ak} = (0,0,0)$. The same feature is displayed in (c) and (d) at the time reversal invariant momenta $\mathbf{ak} = (\pm 1, 0, 0)$. In these plots the parameter values are $t_{d_1} = 1$, $t_{f_1} = -0.7900$, $t_{d_2} = 0.01$, $t_{f_2} = 0.01$, $t_{d_3} = 0.001$, $t_{f_3} = 0.001$, $\epsilon_f = -0.02$, $V = 0.1860$, $|b| = 0.8900$, $\mu = 0$, and $M = 0$. The 3D plot of the spin polarization density (or spin texture) is displayed in (e) using the same parameter values except that $\mu = -0.01$.

$$\langle - | h_{\text{surface}}(k = K_i, M = 0) | - \rangle = \widetilde{E}_k^d(\mu, k) - \vartheta_{z0} = E_- . \quad (17)$$

Obviously enough, $E_- < E_+$. Thus, the occupied state corresponds to the parity eigenvalue -1 . Since the Z_2 invariant is determined by the parity eigenvalue of the occupied state, the extended version of the Anderson model investigated here advocates the strong topological insulator case when $M = 0$. This is in disagreement with the conclusion in refs.[23,24]. However, the finding does agree with the theoretical and experimental observations [2,48- 55] reported earlier.

4. Discussion and concluding remarks

As already stated, the strong correlation effects and diverse surface conditions make a generic TKI system extremely complicated and almost a Gordian knot [4-16,]. Despite this, as we have seen above, our analysis based on a minimalistic model could show that QAH state is accessible in the presence of FM and the model corresponds to a non-trivial topological insulator in the absence of FM. Besides, in order to obtain satisfactory surface band spectrum we found that $|b|^2 \approx 0.80 - 0.90$. The corresponding value of the effective mass is around $250 m_e$ where m_e is the bare mass of an electron. This is in agreement with the experimental finding [43]. The indication is that the signature of the strong correlation in the bulk is large effective mass of the spin-momentum locked carriers on the surface. These are the points significance of the present study. There is, however, a caveat which concerns the fact that we have taken into account only the lowest-order cubic harmonics [54] in the hybridization term in (1). In fact, it is desirable to introduce better odd-parity expressions for this form factor and re-investigate the present problem from a better perspective bringing about some improvement in the surface Hamiltonian. This is expected to facilitate more refined analysis of surface state excitation spectrum including DC feature. Another issue is the heuristic evanescent wave approach made to obtain the surface state Hamiltonian $h_{\text{surface}}(k, \mu, |b|, M = 0)$ following ref.[44]. Instead of this, one may consider a slab geometry for this purpose with the thickness along the z direction. The thickness may be limited in $z \in [-d/2, d/2]$, where d is measure of the penetration depth of surface states. We may further assume the

open/ non-open boundary conditions and investigate the existence / non-existence of surface states. These are some of the essential points which need to be looked into for further refinement.

The Rashba coupling can arise in a system due to the proximity of material lacking in the structural inversion symmetry. In view of the spin-polarized ARPES measurements [53, 56] which appear to confirm the surface helical spin texture [53, 56], it would be interesting to see how does surface state react to Rashba splitting. This problem needs an extensive investigation introducing an additional term representing the Rashba spin-orbit coupling (RSOC) between the d -electrons, viz. $h_z = \left[\left(\frac{1}{2} \right) \left(-\alpha_0 \sin(k_y a) \right) \sigma_x \otimes (\tau_z + \tau_0) + \left(\frac{1}{2} \right) \alpha_0 \sin(k_x a) \sigma_y \otimes (\tau_z + \tau_0) \right]$, in Eq.(7). Here α_0 stands for the strength of RSOC. There are many other complications [5,6,8, 57-62], such as the unusual dichotomy between de Haas-van Alphen(dHvA) and Shubnikov-de Haas (SdH) quantum oscillations [60], to bring home the point that the system needs concerted investigation. There are some contentious issues as well, such as the Hermiticity of an open system is universally lost as the system always involves certain degrees of gain and loss. The ubiquitous electron-electron, electron-impurity, and electron-photon scatterings in an electronic system are responsible for this loss/gain. It is hoped that these issues will motivate the condensed matter physics community to delve deeper into the problem.

In conclusion, looking at the controversies and the possibilities [5,6,8, 57-62], it is anybody's guess that there are many unsettled issues. Unless other TKI candidates are discovered and thoroughly studied, it is perhaps difficult to achieve enhancement in the current understanding of strongly correlated topological insulators. In this backdrop, it is pertinent to make an attempt to investigate thoroughly what exactly are the physical explanation of the issues involved. In a future communication, we shall undertake a part of this demanding task.

References

- 1 D. J. Kim, S.Thomas.; T. Grant, J. Botimer, Z. Fisk, and J.Xia, Sci. Rep., 3, 3150(2013).
2. M. Dzero, K Sun, V. Galitski, P. Coleman, Phys. Rev. Lett., 104, 106408(2010); *ibid* Phys. Rev. B 85, 045130 (2012).
- 3.P. P. Baruselli and M. Vojta, Scanning tunneling spectroscopy and surface quasiparticle interference in models for the strongly correlated topological insulators SmB₆ and PuB₆, Phys. Rev. B 90, 201106 (2014).
4. V. Alexandrov, P. Coleman, O. Erten, Phys. Rev. Lett. 114, 177202 (2015).
5. S. Sen, N. S. Vidhyadhiraja, E. Miranda , V. Dobrosavljevic, and W. Ku, Physical Review Research 2, 033370 (2020).
6. J. Knolle, and N.R. Cooper, Phys. Rev. Lett. 118, 096604 (2017).
7. Erten, O., Chang, P.-Y., Coleman, P. & Tsvelik, A. M., Phys. Rev. Lett. 119, 057603 (2017).
8. D. Chowdhury, I. Sodemann, and T. Sentil, Nat. Commn. 9, 1766 (2018).
9. H.Shen, and L.Fu, Phys. Rev. Lett. 121, 026403 (2018).
10. D. Chowdhury, I. Sodemann, and T Sentil, Nat. Commn. 9, 1766 (2018).

11. H. Pirie, Yu Liu, A. Soumyanarayanan, P. Chen, Y. He, M. M. Yee, P. F. S. Rosa, J. D. Thompson, D.-J. Kim, Z. Fisk, X. Wang, J. Paglione, D. K. Morr, M. H. Hamidian, and J. E. Hoffman, *Nat. Phys.* 16, 52 (2020).
12. R. Peters, T. Yoshida, and N. Kawakami, *Phys. Rev. B* 100, 085124 (2019).
13. W. K. Park, J. A. Sittler, L. H. Greene, W. T. Fuhrman, J. R. Chamorro, S. M. Koohpayeh, W. A. Phelan, and T. M. McQueen, *Phys. Rev B* 103, 155125 (2021).
14. R. Peters, K. Kimura, Y. Michishita, T. Yoshida, and N. Kawakami, *arXiv:2110.04467 [cond-mat.str-el]*; *Phys. Rev. B* 104 (23), 235153(2021).
15. Z. Luo, M. Ferrero, D.-X. Yao, W. Wu, *Phys. Rev. B* 104, L161119(2021).
16. P. Alonso-Cuevillas Ferrer, O. M. Yevtushenko, A. Weichselbaum, *Phys. Rev. Research* 5, 033016 (2023).
17. M. Legner, Topological Kondo insulators: materials at the interface of topology and strong correlations (Doctoral Thesis), ETH Zurich Research Collection (2016). Link: <https://www.research-collection.ethz.ch/bitstream/handle/20.500.11850/155932/eth-49918-02.pdf?isAllowed=y&sequence=2>.
18. A. Sharma, H. Yan, L. Zhang, X. Sun, X. B. Liu, Y. Lu, Highly enhanced many-body interactions in anisotropic 2D semiconductors. *Accounts of Chemical Research*, 51(5):1164–1173 (2018).
19. C. M. Wang, Hai-Peng Sun, Hai-Zhou Lu, and X. C. Xie, *Phys. Rev. Lett.* 119, 136806 (2017).
20. S. Wolgast, C. Kurdak, K. Sun, J. W. Allen, D.-J. Kim, and Z. Fisk, Low-temperature surface conduction in the Kondo insulator SmB_6 , *Phys. Rev. B* 88, 180405 (2013).
21. Feng Lu, J.Z. Zhao, H. Weng, Z. Fang, and Xi Dai, *Phys. Rev. Lett.* 110, 096401 (2013).
22. D. J. Kim, J. Xia, and Z. Fisk, “Topological surface state in the Kondo insulator samarium hexaboride,” *Nature Materials* 13, 466 (2014).
23. A. P. Sakhya and K.B. Maiti, *Scientific Reports* volume 10, Article number: 1262 (2020).
24. P. Hlawenka, K. Siemensmeyer, E. Weschke, *et al.*, Samarium hexaboride is a trivial surface conductor. *Nat Commun* 9, 517 (2018). <https://doi.org/10.1038/s41467-018-02908-7>
25. P. K. Biswas, M. Legner, G. Balakrishnan, M. C. Hatnean, M. R. Lees, D. M. Paul, E. Pomjakushina, T. Prokscha, A. Suter, T. Neupert, *et al.*, *Phys. Rev. B* 95, 020410 (2017).
26. L. Fu, C.L. Kane.: Time reversal polarization and a Z_2 adiabatic spin pump. *Phys. Rev. B* 74, 195312 (2006).
27. L. Fu, C. L. Kane, and E.J. Mele: Topological insulators in three dimensions. *Phys. Rev. Lett.* 98, 106803 (2007).
28. C. L. Kane, and E.J. Mele: Z_2 Topological Order and the Quantum Spin Hall Effect. *Phys. Rev. Lett.* 95, 146802 (2005).
29. G. Li, Z. Xiang, F. Lu, T. Asaba, B. Lawson, P. Pal, C. Tinsman, A. Berkley, S. Wolgast, and L. Lu, Two-dimensional Fermi surfaces in Kondo insulator SmB_6 , *Science* 346, 1208–1212 (2014).
30. R. Yu, H. Weng, X. Hu, Z. Fang, and X. Dai, *New J. Phys.* 17, 023012 (2015).
31. M. Legner, A. Rüegg, and M. Sigrist, Surface-state spin textures and mirror Chern numbers in topological Kondo insulators, *Phys. Rev. Lett.* 115, 156405 (2015).
32. M. Legner, A. Rüegg, and M. Sigrist, *Physical Review B* 89, 085110 (2014).
33. J. Kim, K. Kim, C.-J. Kang, S. Kim, H. C. Choi, J.-S. Kang, J. D. Denlinger, and B. I. Min, *Phys. Rev. B* 90, 075131 (2014).
34. T. Takimoto, *J. Phys. Soc. Jpn.* 80, 123710 (2011).
35. J. Werner and F. F. Assaad, *Phys. Rev. B* 88, 035113 (2013); *ibid.* *Phys. Rev. B* 89, 245119 (2014).
36. D. K. Efimkin and V. Galitski, *Phys. Rev. B* 90, 081113(R)(2014).

37. B. Gorshunov, N. Sluchanko, A. Volkov, M. Dressel, G. Knebel, A. Loidl, and S. Kunii, *Phys. Rev. B* **59**, 1808 (1999).
38. P. Phillips. *Advanced Solid State Physics*. Cambridge University Press, (2012).
39. Udai Prakash Tyagi, Kakoli Bera and Partha Goswami, On Strong f -Electron Localization Effect in a Topological Kondo Insulator, *Symmetry*, **13**(12), 2245 (2021).
40. B.S.Tan et al., Unconventional Fermi surface in an insulating state. *Science* **349**, 287–290 (2015).
41. M. Hartstein, W. H. Toews, and Suchitra E. Sebastian, Fermi surface in the absence of a Fermi liquid in the Kondo insulator SmB₆, *Nature Physics* volume **14**, pages 166–172 (2018).
42. X.-Y. Feng, J. Dai, C.-H. Chung, and Q. Si, *Phys. Rev. Lett.* **111**, 016402(2013).
43. H. Pirie et al., Imaging emergent heavy Dirac fermions of a topological Kondo insulator, *Nat. Phys.* **16**, 52–56 (2020).
44. J Betancourt, S. Li, X. Dang, J. D. Burton, E. Y. Tsymbal, and J. P. Velev, *J. Phys.: Condens. Matter* **28** 395501(2016).
45. Y. Zhang, C.-X. Liu, X.-L. Qi, X. Dai, Z. Fang, and S.-C. Zhang, Topological insulators in Bi₂Se₃, Bi₂Te₃ and Sb₂Te₃ with a single Dirac cone on the surface, *Nat. Phys.* **5** 438 (2009).
46. X.-L. Qi, Y.-S. Wu, and S.-C. Zhang, Topological quantization of the spin hall effect in two-dimensional paramagnetic semiconductors, *Phys. Rev. B* **74**, 085308 (2006).
47. X.-L. Qi and S.-C. Zhang, Topological insulators and superconductors, *Reviews of Modern Physics* **83**, 1057 (2011).
48. There should be a surface Dirac cone or at least a Kramers degeneracy at $k=0$. See for comparison the Dirac cone topological surface states at TRIMS calculated by DFT F. Lu, J. Zhou, Zhao, H. Weng, Z. Fang, Xi Dai *Phys. Rev. Lett.* **110**, 096401 (2013).
49. W. Ruan, C. Ye, M. Guo, F. Chen, X. Chen, G.-Ming Zhang, and Y. Wang, *Phys. Rev. Lett.* **112**, 136401(2014).
50. S. Rößler, T.-Hwan Jang, D.-Jeong Kim, and S. Wirth, *Proc. Natl. Acad. Sci. U.S.A.*, **111** (13) 4798 (2014). <https://doi.org/10.1073/pnas.1402643111>.
51. Neupane, M., Alidoust, N., Xu, S.Y. *et al.* Surface electronic structure of the topological Kondo-insulator candidate correlated electron system SmB₆. *Nat Commun* **4**, 2991 (2013). <https://doi.org/10.1038/ncomms3991>.
52. Jiang, J., Li, S., Zhang, T. *et al.* Observation of possible topological in-gap surface states in the Kondo insulator SmB₆ by photoemission. *Nat Commun* **4**, 3010 (2013). <https://doi.org/10.1038/ncomms4010>.
53. N. Xu, P. K. Biswas, J. H. Dil, G. Landolt, S. Muff, C. E. Matt, X. Shi, N. C. Plumb, M. Radavic, E. Pomjakushina, K. Conder, A. Amato, S. V. Borisenko, R. Yu, H.-M. Weng, Z. Fang, X. Dai, J. Mesot, H. Hing, and M. Shi, “Direct observation of the spin texture in SmB₆ as evidence of the topological Kondo insulator,” *Nature Comm.* **5**, 4566 (2014). <https://doi.org/10.1038/ncomms5566>.
54. M. Dzero, J. Xia, V. Galitski, and P. Coleman, “Topological Kondo Insulators,” *Annual Review of Condensed Matter Physics* **7**, 249–280 (2016).
55. Y. Ohtsubo et al., Non-trivial surface states of samarium hexaboride at the (111) surface. *Nat. Commun.* **10**, 2298 (2019). This paper reports the first direct observation of spin-textured surface states for a SmB₆ surface other than the natural (100) cleavage plane.
56. S. Suga et al., *J. Phys. Soc. Jpn* **83**, 014705 (2014).
57. W.T.Fuhrman, J.R. Chamorro, P. Alekseev *et al.*, Screened moments and extrinsic in-gap states in samarium hexaboride. *Nat Commun* **9**, 1539 (2018).
58. M. E. Boulanger et al., *Phys. Rev. B.* **97**, 245141 (2018).
59. M. Orendáč, et al. *Phys. Rev. B* **96**, 115101 (2017).

60. A.Panda, S.Banerjee, and M.Randeria, Proceedings of National Academy of Sciences, 119 (42) e2208373119 (2022).

61. N. Harrison, Highly asymmetric nodal semimetal in bulk SmB6. Phys. Rev. Lett. 121, 026602 (2018).

62. M. Abele et al., Topological nonmagnetic impurity states in topological Kondo insulators, Phys. Rev. B 101, 094101 (2020).

Appendix A

The bulk eigenstates corresponding to the eigenvalues in (4) are given by

$$|u_n(k_x, k_y, k_z)\rangle = \frac{1}{N_n^{1/2}} \begin{pmatrix} 1 \\ -\frac{\vartheta_z}{A} \\ \frac{2M\vartheta_z}{B_n(k)} \\ -C_n(k) \\ AB_n(k) \end{pmatrix}, n=1, 2,3,4, A = (\vartheta_x - i\vartheta_y) \quad (\text{A.1})$$

$$B_n(k) = (\vartheta_x^2 + \vartheta_y^2 + \vartheta_z^2) - (E_n - \widetilde{E}_k^d(\mu, k) + M)(E_n - \widetilde{E}_k^f(\mu, k)), \quad (\text{A.2})$$

$$C_n(k) = (E_n - \widetilde{E}_k^d(\mu, k) + M) \vartheta_z^2 + (E_n - \widetilde{E}_k^d(\mu, k) - M)(\vartheta_x^2 + \vartheta_y^2) \\ + ((E_n - \widetilde{E}_k^d(\mu, k))^2 - M^2) (E_n - \widetilde{E}_k^f(\mu, k)), \quad (\text{A.3})$$

$$N_n = (1 + \frac{\vartheta_z^2}{A^*A} + \frac{4M^2\vartheta_z^2}{B_n^2(k)} + \frac{C_n^2(k)}{A^*AB_n^2(k)}). \quad (\text{A.4})$$

Appendix B

We first write the eigenstates linked to the eigenvalues in (10) in a general manner as

$$|u^{(j)}(k)\rangle = \frac{1}{N_j^{1/2}} \begin{pmatrix} \psi_1^j(k) \\ \psi_2^j(k) \\ \psi_3^j(k) \\ \psi_4^j(k) \end{pmatrix}, j=5, 6,7,8, \quad (\text{B.1})$$

where $N_j = [\psi_1^{j*}(k)\psi_1^j(k) + \psi_2^{j*}(k)\psi_2^j(k) + \psi_3^{j*}(k)\psi_3^j(k) + \psi_4^{j*}(k)\psi_4^j(k)]$. Next, we define an operator s^μ in terms of the Pauli matrices σ^μ as

$$s^\mu = \begin{pmatrix} \sigma^\mu & 0 \\ 0 & -(\sigma^\mu)^* \end{pmatrix}. \quad (\text{B.2})$$

The spin polarization density in the z-direction for the j^{th} band is given by

$$\rho_j^z = \langle u^{(j)}(\mathbf{k}) | s^z | u^{(j)}(\mathbf{k}) \rangle . \quad (\text{B.3})$$

We obtain

$$\rho_j^z = N_j^{-1} [\psi_1^{j*}(k) \psi_1^j(k) - \psi_2^{j*}(k) \psi_2^j(k) - \psi_3^{j*}(k) \psi_3^j(k) + \psi_4^{j*}(k) \psi_4^j(k)] . \quad (\text{B.4})$$